X-ray photoelectron diffraction study of Cu(1 1 1): Multiple scattering investigation

L. Despont [a,*], D. Naumović [b], F. Clerc [a], C. Koitzsch [a], M.G. Garnier [a], F.J. Garcia de Abajo [c], M.A. Van Hove [d], P. Aebi [a]

[a] *Institut de Physique, Université de Neuchâtel, Rue A.-L. Breguet 1, CH-2000 Neuchâtel, Switzerland*
[b] *Institut de Physique, Université de Fribourg, Pérolles, CH-1700 Fribourg, Switzerland*
[c] *Centro Mixto CSIC-UPV/EHU, 20080 San Sebastián, Spain*
[d] *Department of Physics and Materials Science, City University of Hong Kong, 83 Tat Chee Avenue, Kowloon, Hong Kong*

Abstract

Multiple scattering theory based on a cluster model is used to simulate full-hemispherical X-ray photoelectron diffraction measurements in order to verify how state of the art multiple scattering simulations are able to reproduce the experiment. This approach is applied to the Cu(1 1 1) surface for two different photoelectron kinetic energies. Differences and similarities between single and multiple scattering are discussed in comparison with experimental results. We find that the present approach gives very good results despite some limitations.

Keywords: Photoelectron diffraction; Multiple scattering; Copper; Electron solid interaction; Scattering; Diffraction

1. Introduction

The complete knowledge of the atom positions is a necessary prerequisite for the understanding of the various properties of material's surfaces. Among the numerous techniques available to the scientist to obtain this crystalline information, X-ray photoelectron diffraction (XPD) has proven to be very powerful, owing to its chemical sensitivity and its ability to measure sub-angstrom atomic displacements. However without theoretical simulations it is often difficult to understand the different structures appearing in XPD data and to link them to true crystalline positions. Single-scattering codes are used for some time now to simulate diffractograms and are sufficient to calculate the major crystalline structure, the orientation of adsorbed molecules [1], or to optimize atom positions of submonolayer coverages of adatoms via a *R*-factor analysis [2]. However, this approach appears insufficient for multilayer systems like in ferroelectric films or for surface termination determination of quasi-two-dimensional systems [3], for which the multiple scattering approach becomes essential.

Recently, thanks to the development of new computer codes and the availability of faster computers, it has become possible to simulate XPD diffractograms using a MSC formalism (see Ref. [4] and references therein). It is the aim of this paper to perform an as complete as possible comparison of Cu(1 1 1) surface XPD measurements with the MSC simulations using the EDAC (electron diffraction in atomic clusters) computer code [4]. Therefore, this study serves to verify to what degree state of the art EDAC multiple scattering simulations are able to reproduce full-hemispherical XPD patterns.

---

* Corresponding author.
  E-mail address: laurent.despont@unine.ch (L. Despont).

2. Experimental and computational details

The XPD measurements are performed in a modified vacuum generators ESCALAB Mark II X-ray photoelectron spectrometer equipped with a fixed hemispherical electron energy analyzer, and a three channeltron detection system, operated with a base pressure in the lower 10^{-11} mbar region. The X-ray tube contains a MgKα ($h\nu = 1253.6$ eV) and SiKα ($h\nu = 1740$ eV) twin anode. The samples are fixed on a computer-controlled two-axis goniometer capable of scanning the emission angle over the full hemisphere above the surface [5–10]. Data has been collected for a polar angel range $\theta \in [0°, 78°]$ and an azimuthal angle range $\phi \in [0°, 360°]$.

For electron kinetic energies higher than approximately 500 eV the analysis of diffraction patterns is made easier by the so-called "forward focusing" effect which consists in an enhancement of the emission intensity along densely packed atomic planes and rows of atoms (corresponding to low-index crystallographic directions) [11]. In the above-mentioned energy range, the photoelectron inelastic mean free path (λ) is large and thus the number of scattering events can be also large. The scattering on the first few atoms has a tendency to focus the emission in the emitter–scatterer direction while on the subsequent atoms it tends to defocus the signal [12]. It is a clear indication for the necessity to use MSC in order to get precise information on the intensity and shape of the "forward focusing" peaks. Furthermore, the defocusing is also linked to the development of the conventional Kikuchi bands which become more intense when the forward-scattering peak intensity diminishes [12]. Thus MSC is also required to reproduce Kikuchi band intensities as well as diffraction pattern structure details. Single-scattering (SSC) is well-known to overemphasize the intensity of the "forward focusing" peaks [11].

The cluster-model approach of the EDAC code [4] used here to simulate the XPD experiment is based on the muffin-tin potential approximation [13]. EDAC evaluates the MSC expansion using a fully convergent recursion method. In order to overcome the rapidly-growing computational demand, EDAC contains the Rehr and Albers [14] procedure consisting in a separable representation of the free-electron Green function. The Haydock recursion method is used to calculate an iterative solution of the MSC series. The computation time needed to determine the scattered wave function is proportional to $nN^2(l_{max} + 1)^3$, where n is the scattering order, N the number of atoms used in the cluster and l_{max} the maximum angular momentum quantum number. This last parameter permits an approximation of the outgoing photoelectron wave function using a combination of l_{max} spherical harmonics. The number of spherical harmonics is approximately given by $l_{max} \approx k r_{mt}$ [13] where k is the photoelectron wave vector and r_{mt} the muffin-tin radius. By estimating an average nearest-neighbour distance and selecting a photoelectron kinetic energy E_{kin}, the l_{max} parameter can roughly be deduced.

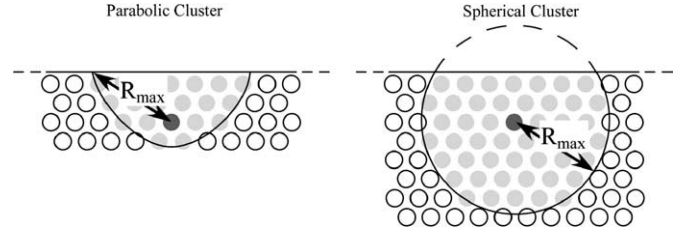Fig. 1. Cluster shapes as a function of R_{max}. The light and dark gray disks correspond to scatterers and to the emitter, respectively.

The number N of scattering atoms in the cluster is defined with the parameter R_{max}. Fig. 1 shows how R_{max} defines the scattering volume using the emitter either as the focus of a parabola or as a sphere center. The following R_{max} values are chosen: $R_{max} = 22$ Å for $E_{kin} = 807.2$ eV (Cu 2p$_{3/2}$ core level excited with SiKα) and $R_{max} = 13$ Å for $E_{kin} = 320.8$ eV (Cu 2p$_{3/2}$ core level excited with MgKα). To increase the contribution of scattering of the atoms located between the emitters and the surface, the parabolic shape is selected in the present study, which gives a scattering volume containing approximately 300 atoms for the high energy case and 100 atoms for the low energy one. The electron inelastic mean free path λ can be deduced from the universal relationship between kinetic energy and inelastic mean free path, given by [15,16]

$$\lambda(\text{Å}) = \frac{538 \cdot d}{E_{kin}^2(\text{eV})} + 0.13 \cdot \sqrt{d^3 \cdot E_{kin}(\text{eV})}, \quad (1)$$

where d is the Cu(1 1 1) interlayer spacing ($d = 3.6149 \cdot \frac{1}{\sqrt{3}}$ Å). In the case of photoelectrons with $E_{kin} = 807.2$ eV, $\lambda \approx 11$ Å, nine emitters distributed down to -16.7 Å below the surface are chosen. At lower photoelectron kinetic energy, $E_{kin} = 320.8$ eV with $\lambda \approx 7$ Å, five emitters distributed over five layers are chosen down to -8.3 Å. The introduction of an inner potential V_0 permits to consider the refraction of the photoelectron wave at the surface-potential step. For Cu, $V_0 = 13.5$ eV is taken [13]. The calculations were performed for a temperature $T = 300$ K and thermal vibrations are introduced by means of a reasonable non-zero Debye temperature θ_D. Best agreement between experiment and MSC theory is obtained by optimizing l_{max}, R_{max}, θ_D, n and the number of emitters.

To obtain a quantitative value of the agreement between calculated and measured diffractograms, an R-factor analysis based on the multipole expansion of the angular intensity distribution, i.e., the expansion into spherical harmonics, has been used. The R_{MP}-factor calculation method is detailed in Ref. [2].

3. Results and discussion

The calculated and measured diffractograms of Cu(1 1 1) 2p$_{3/2}$ measured with SiKα ($E_{kin} = 807.2$ eV) are presented in Fig. 2, using the same linear gray scale and stereographic
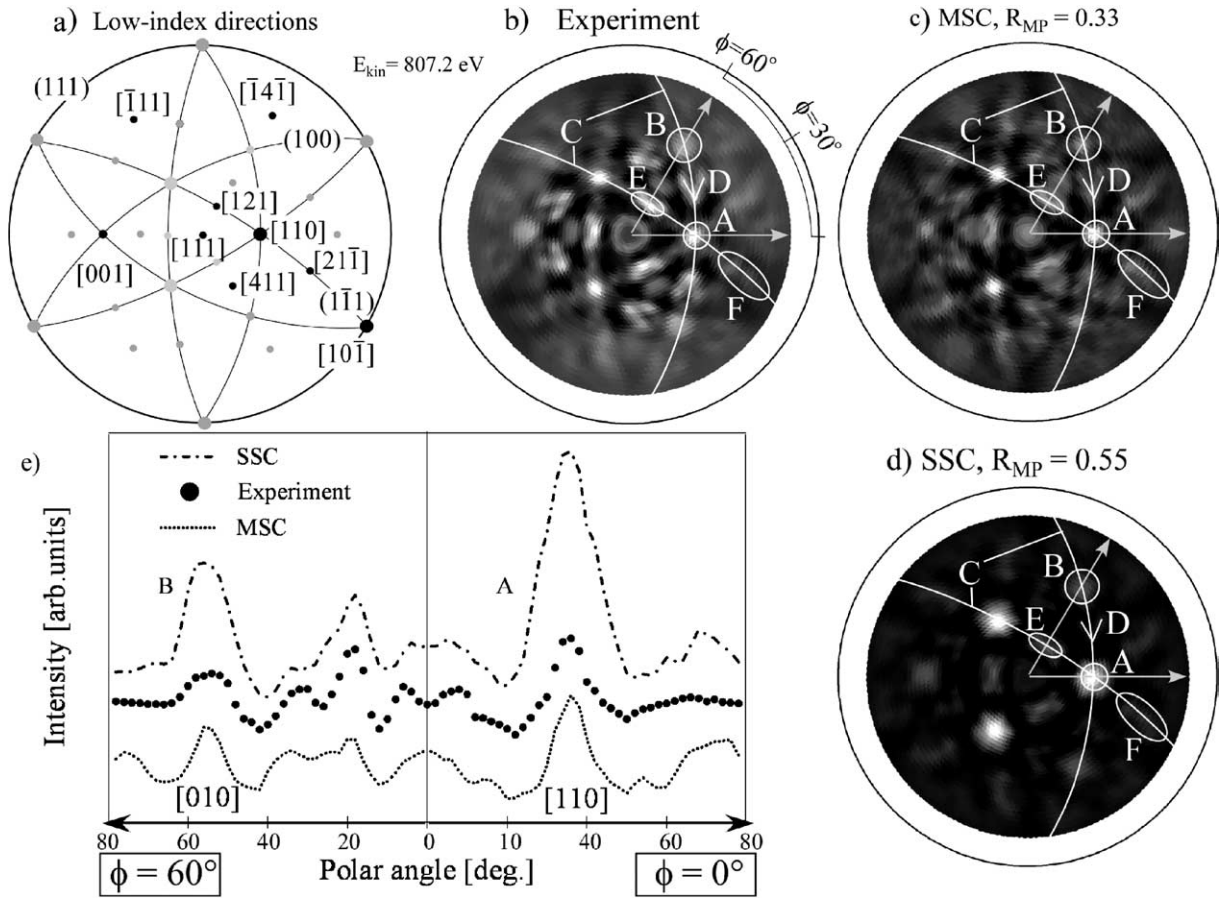
Fig. 2. Stereographic projections for Cu(1 1 1). (a) The projections of some low-index crystal planes (lines) and the major directions (dots) are drawn in order to facilitate the discussion. The labeled low-index directions are indicated by black dots. Stereographic projections of (b) measured and (c), (d) multiple and single-scattering simulated diffractograms for Cu 2p$_{3/2}$ at 807.2 eV (SiKα, hv = 1740 eV). (e) Polar scans at ϕ = 60° and 0°. The experimental profiles are represented by black dots. Polar scans are normalized with respect to their mean intensity and offset with respect to each other.

projection. Experimental diffractograms are acquired simultaneously at two different kinetic energies: one exactly at the center of the 2p$_{3/2}$ photoemission line (E_{kin} = 807.2 eV in this case) and one slightly above (E_{kin} = 812.2 eV) to monitor the background intensity variation. The subtraction of the second from the first diffractogram, taking into account the channeltron sensitivities, allows to get rid of the inelastic electron background. Taking advantage of the threefold symmetry of the Cu(1 1 1) the measured diffractograms are azimuthally averaged. In order to facilitate the comparison with the calculation, a smooth polar angle dependent background is subtracted from both the measured and the calculated diffractograms. This polar angle dependent background originates from three different effects. First, the analyzed surface area changes with 1/cos(theta) by scanning the polar angle (theta) from normal emission (theta = 0°) to grazing emission (theta = 78°, here). Secondly, due to the refraction at the surface (linked to the inner potential), the photoelectron intensity is anisotropically reduced with larger polar angles. And finally, the photoelectron intensity depends on the photoelectron escape depth, which is a function of the polar angle. The removal of a polar angle dependent background therefore permits to obtain a

diffractogram independent of these aspects, emphasizing the features due to interference.

Fig. 2a shows the stereographic projection of the low-index crystal planes and directions. In all the theoretical and experimental data, see Fig. 2b–d, the "forward focusing" peaks along ⟨1 1 0⟩ directions are dominant (label "A" in Fig. 2b–d), and those along the ⟨0 0 1⟩ directions are less intense (B). The shapes and widths of these two features are better reproduced by the MSC calculation than by the SSC, as can be seen in Fig. 2e. Kikuchi bands representing {1 0 0} and {1 1̄ 1} type planes (C) are present in MSC with a width and intensity comparable to the experiment while they appear broader in SSC. The same V-like structure (D) is observed in all diffractograms on the {1 0 0} Kikuchi bands between the dominant ⟨1 1 0⟩ peaks and the ⟨0 0 1⟩ directions. Again, this experimental V-like feature is better reproduced by the MSC code. Interferences of two neighbouring ⟨1 1 0⟩ directions generate modulations along the 1 1̄ 1 planes with maxima near [1 2 1] (E) [6]. Similar features (F) appear in the [2 1 1̄] direction along the same planes, produced by interferences of the scattering by [1 1 0] and invisible [1 0 1̄] neighbours. The E and F modulations are roughly the same for the experiment, MSC and

SSC simulations. So far MSC has given very good results. However, the experimental diffractogram on Fig. 2b exhibits a doughnut-like feature in the center which is not reproduced in the calculation. In fact, SSC gives a better agreement (see Fig. 2e at 0°). By changing $l_{\max}$, the number of spherical harmonics taken into account, this feature can be reproduced in the MSC simulation but at the expense of disagreement in other diffractogram structures, leading to an increase of the below-discussed R-factor. This points to a possible instability with respect to the $l_{\max}$ convergence.

In order to give a more quantitative comparison between measurement and calculations, and especially between MSC and SSC, two polar cuts at $\phi = 60°$ and $0°$ are displayed (Fig. 2e), for the measured and calculated Cu $2p_{3/2}$ diffractograms. All polar cuts are normalized with respect to their mean intensity and offset with respect to each other. The most striking difference between the two calculations lies in the "forward focusing" peaks, (label A and B), whose intensities is much better reproduced by MSC calculation. As already mentioned, this overemphasizing of the "forward focusing" peaks is a well-known shortcoming of SSC. What is visible locally in the interference patterns is confirmed by a global match approach which uses the reliability R_{MP}-factor to judge the quality of the fit between the complete experimental interference pattern data and theory. The much smaller value for MSC, $R_{\mathrm{MP}} \approx 0.33$, than for SSC, $R_{\mathrm{MP}} \approx 0.55$, confirms the better global agreement obtained with MSC [1] and confirms what has been obtained by eye. Note that the better agreement is not only due to the overemphasized "forward focusing" peaks with the SSC approach but also due to better agreement with the small structures comparing the MSC and the experimental result. This has been checked by artificially putting the intensities in the "forward focusing" areas to a common mean value. The idea is to remove the contribution of the overemphasized "forward focusing" peaks in the SSC to the R-factor. The obtained R-factor for the SSC approach is still worse than for MSC, indicating that the "forward focusing" peaks are not the only reason of the better agreement between the experiment and MSC.

This conclusion is corroborated with the result of the following analysis using a smaller photoelectron energy. In fact, the same $2p_{3/2}$ photoelectron line is selected, but excited with MgKα radiation ($hv = 1253.6$ eV), changing the photoelectron kinetic energy to 320.8 eV. MSC effects are damped owing to the shorter inelastic mean free path λ, which still corresponds to 2–3 atomic distances. In this case, the SSC model should perform better than at high photoelectron kinetic energy.

The same procedure in terms of data treatment as for the high kinetic energy has been used in order to facilitate the comparison between both energies. In Fig. 3, the intensity enhancements along $\langle 110 \rangle$ directions are still domi-

nant (label A$'$), as in the true "forward focusing" regime at high kinetic energies. These peaks correspond to scattering on nearest-neighbour atoms. Nevertheless, the signal is broader at lower kinetic energy, because the photoelectron scattering amplitudes become more isotropic. In the SSC calculation this enlargement is too prominent owing to the absence of defocusing [12]. At the diffractogram center, the intensity modulation (E) in Fig. 2 has been replaced by a mushroom-shaped feature (B$'$), with a higher intensity area on the top. Its shape and width are well reproduced in the MSC simulation. The C$'$ structure, which was a "forward focusing" peak at higher kinetic energy, is now broader. It has a V-like shape with a small asymmetry visible in the measured and SSC interference patterns, originating from photon polarization effects owing to the oblique photon incidence in our setup. These asymmetry effects are especially visible at lower energies [6]. Presently, our special setup geometry and therefore this asymmetry behaviour cannot be simulated with EDAC. Finally, the shapes and intensities of the D$'$ and E$'$ regions are globally the same between experimental data and theory. Two polar cuts at $\phi = 60°$ and $0°$ are displayed in Fig. 3d. The A$'$ and C$'$ peaks, corresponding to nearest-neighbour emitter–scatterer directions, are well described with the MSC approach, as well as the more complex B$'$ feature. For the specific polar scan, MSC does not appear better than SSC. In particular, the center part of feature A$'$ in the experiment has a narrowness which is not reproduced in both calculations. Note that features in a localized angle-range may be better reproduced by choosing a different set of parameters but this results in a worse global agreement with a higher R-factor.

Despite the polarization effect not being taken into account by MSC, the R_{MP}-factor analysis performed on the diffractograms displayed in Fig. 3 shows a better agreement between experiment and calculation using the MSC ($R_{\mathrm{MP}} \approx 0.45$)[2] than SSC ($R_{\mathrm{MP}} \approx 0.50$), confirming the importance to use a multiple scattering formalism to simulate diffractograms.

For a more detailed comparison of the agreement between the experiment and both calculation methods and for both kinetic energy cases, the local anisotropy, $A = \frac{I(\theta, \phi) - I_{\min}}{I_{\max}}$, is calculated for different features, as well as for the total diffractogram, and is reported in Table 1. The anisotropy does not give information about similarities in the shape of particular features in the different cases (MSC, experiment, SSC) but indicates the intensity variations only. First, the anisotropy has been calculated for the entire MSC, SSC and experimental diffractograms, for both $E_{\mathrm{kin}} = 807.2$ eV and $E_{\mathrm{kin}} = 320.8$ eV cases. In the high kinetic energy case, as shown on the left part of Table 1, the anisotropy of the full experimental diffractogram (55%) is more similar to the one for MSC (68%) than to the one for SSC (84%) due to the overemphasized

---

[1] The parameters used are $l_{\max} = 8$ and $\theta_D = 50$.

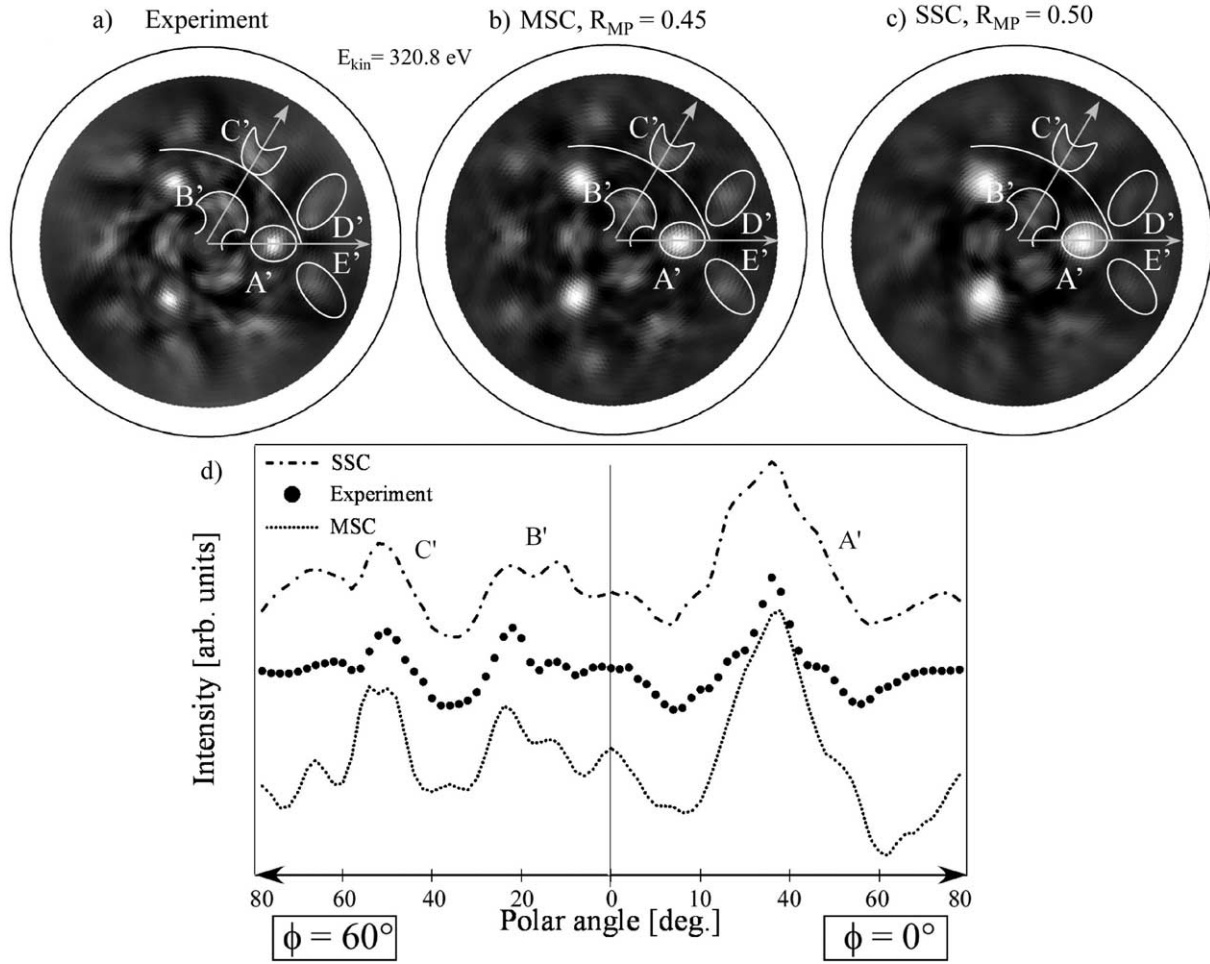[2] The parameters used are $l_{\max} = 13$ and $\theta_D = 150$.

Fig. 3. Stereographic projections of (a) measured, (b) MSC calculated and (c) SSC simulated diffractograms for Cu $2p_{3/2}$ at 320.8 eV. (d) Polar scans as labeled.

Table 1
Anisotropies calculated on different diffractogram regions for both kinetic energy cases (Figs. 2 and 3)

Region	A (E_{kin} = 807.2 eV)			Region	A (E_{kin} = 320.8 eV)		
	SSC	Exp	MSC		SSC	Exp	MSC
Entire diffractogram	84%	55%	68%	idem	63%	49%	76%
A	66%	39%	47%	A′	48%	40%	52%
B	44%	21%	34%	C′	30%	22%	45%
D	63%	40%	33%	D′	35%	24%	50%
F	56%	22%	39%	E′	41%	28%	50%
Circle ($0 \leqslant \theta < 30°$)	44%	21%	34%	idem	52%	38%	59%

"forward focusing" peak intensities in the latter case. For the same reason, the anisotropy values of the A and B labeled regions are more similar comparing experiment with MSC than comparing with SSC. Also, a comparable observation can be done for the two Kikuchi band modulations labeled with D and F. Globally, smaller anisotropies were obtained for the experiment and the MSC while the SSC pattern regions always show much larger anisotropy values in the high kinetic energy case. However it is the opposite in the lower energy case, right part of the Table 1, and especially in regions sensitive to photon polarization effects owing to the oblique photon incidence, namely the C′, D′, E′

labeled regions but with a less dramatic difference in the entire diffractogram. Indeed, the anisotropy values of these features in the SSC are closer to experimental anisotropies than the ones calculated with MSC. However, for the A′ labeled region as well as for the diffractogram center (around the normal emission) the SSC and MSC anisotropies are comparable.

This comparison, using the anisotropy, between both calculation methods gives complementary information about the intensity agreement of local features and complete the feature shape analysis performed above(R_{MP}-factor).

4. Conclusion

In the presented diffractograms, diffraction patterns are dominated by the "forward focusing" peaks along low-index crystallographic directions for both photoelectron kinetic energies. For the higher energy pattern, the relative intensities of "forward focusing" peaks are perfectly reproduced using the MSC code EDAC. Kikuchi bands and less intense peaks are also well simulated and appear with the same width and intensity in the experiment as in MSC. However, a specific doughnut shaped feature close to normal emission is not reproduced for the simulation with the best R-factor. For the lower energy pattern the "forward focusing" is less well reproduced and the difference between MSC and SSC is not as drastic. Nevertheless, for both energies, the lowest R-factors were obtained for MSC simulations, indicating the best match with experimental diffractograms. It appears that it is possible to have a good match in a limited angular range with worse agreement on the global pattern. Therefore, in order to judge a particular parameter set, the capabilities of an algorithm or simulation program, it is of prime importance to test is on an as extended as possible data set. Note that remaining inadequacies of the MSC description are certainly related to the fact that presently it is not possible to converge all available parameters simultaneously, because of memory and CPU requirements. Furthermore, if certain parameters are pushed too far, the algorithms may become numerically unstable. In general, calculations using MSC prove to be necessary to accurately simulate experimental interference patterns and increase the confidence in theoretical results, specially in peak widths and intensities. Such agreement cannot be achieved with SSC calculation.

References

[1] R. Fasel, P. Aebi, R.G. Agostino, D. Naumović, J. Osterwalder, A. Santaniello, L. Schlapbach, Orientation of adsorbed C_{60} molecules determined via X-ray photoelectron diffraction, Phys. Rev. Lett. 76 (25) (1996) 4733–4736.

[2] R. Fasel, P. Aebi, J. Osterwalder, L. Schlapbach, R.G. Agostino, G. Chiarello, Local structure of c(2×2)-Na on Al(001): Experimental evidence for the coexistence of intermixing and on-surface adsorption, Phys. Rev. B 50 (19) (1994) 14516–14524.

[3] Laurent Despont et al., to be published.

[4] F.J. Garcia de Abajo, M.A. Van Hove, C.S. Fadley, Multiple scattering of electrons in solids and molecules: A cluster-model approach, Phys. Rev. B 63 (2001) 075404–1–16.

[5] J. Osterwalder, T. Greber, A. Stuck, L. Schlapbach, Experimental full-solid-angle substrate photoelectron-diffraction data at 1-keV energies: implications for photoelectron holography, Phys. Rev. B 44 (24) (1991) 13764–13767.

[6] D. Naumović, A. Stuck, T. Greber, J. Osterwalder, L. Schlapbach, Full-hemispherical photoelectron-diffraction data from Cu(001): energy dependence and comparison with single-scattering-cluster simulations, Phys. Rev. B 47 (12) (1993) 7462–7479.

[7] R. Fasel, P. Aebi, J. Osterwalder, L. Schlapbach, Direct structural information from X-ray photoelectron diffraction: intermixing and on-surface adsorption of Na on Al surfaces, Surf. Sci. 331–333 (1995) 80–87.

[8] J. Osterwalder, P. Aebi, R. Fasel, D. Naumović, P. Schwaller, T. Kreutz, L. Schlapbach, T. Abukawa, S. Kono, Angle-scanned photoelectron diffraction, Surf. Sci. 331–333 (1995) 1002–1014.

[9] D. Naumović, J. Osterwalder, A. Stuck, P. Aebi, L. Schlapbach, Growth of Au on Cu(001) studied by full hemispherical photoelectron diffraction, Surf. Sci. 287–288 (1993) 950–954.

[10] T. Greber, J. Osterwalder, D. Naumović, A. Stuck, S. Hüfner, L. Schlapbach, Auger electron and photoelectron angular distributions from surfaces: importance of the electron source wave, Phys. Rev. Lett. 69 (13) (1992) 1947–1950.

[11] C.S. Fadley, Synchrotron Radiation Research: Advances in Surface Science, Plenum, New York, 1990.

[12] H.A. Aebischer, T. Greber, J. Osterwalder, A.P. Kaduwela, D.J. Friedman, G.S. Herman, C.S. Fadley, Material dependence of multiple-scattering effects associated with photoelectron and Auger electron diffraction along atomic chains, Surf. Sci. 239 (1990) 261–264.

[13] J.B. Pendry, Low Energy Electron Diffraction, Academic Press, London, 1974.

[14] J.J. Rehr, R.C. Albers, Scattering-matrix formulation of curved-wave multiple scattering theory: application to X-ray absorption fine structure, Phys. Rev. B 41 (12) (1990) 8139–8149.

[15] M.P. Seah, W.A. Dench, Quantitative electron spectroscopy of surfaces: a standard data base for electron inelastic mean free paths in solids, Surf. Interface Anal. 1 (1) (1979) 2–11.

[16] R.E. Ballard, Empirical mean free path curves for electron scattering in solids, J. Electron Spectrosc. Relat. Phenom. 25 (1) (1982) 75–78.